Neuroligin 1 induces blood vessel maturation by cooperating with the α6 integrin.

Samarelli AV,Riccitelli E,Bizzozero L,Silveira TN,Seano G,Pergolizzi M,Vitagliano G,Cascone I,Carpentier G,Bottos A,Primo L,Bussolino F,Arese M

Neuroligin 1 induces blood vessel maturation by cooperating with the ?6 integrin.

THE JOURNAL OF BIOLOGICAL CHEMISTRY (2014) 289

DOI: 10.1074/jbc.M113.530972

Neuroligin 1 Induces Blood Vessel Maturation by Cooperating with the α6 Integrin*

Anna Valeria Samarelli‡,§[1], Elena Riccitelli‡,§, Laura Bizzozero‡,§,Tatiana Nunes Silveira‡,§[2], Giorgio Seano‡,¶[3], Margherita Pergolizzi‡,§,Grazia Vitagliano‡,§, Ilaria Cascone‖, Gilles Carpentier‖, Alessia Bottos‡,§[4],Luca Primo‡,¶, Federico Bussolino‡,**[5] and Marco Arese‡,§[56]

Author Affiliations

1. From the Department of ‡Oncology, University of Torino Medical School,
2. §Laboratory of Neurovascular Biology,
3. ¶Cell Migration, and
4. **Vascular Oncology, Candiolo Cancer Institute, 10060 Candiolo (TO) Italy and
5. the ‖Laboratoire CRRET, Faculté des Sciences et Technologie, Université Paris Est Créteil Val de Marne, 61 avenue du Général de Gaulle, 94010 Créteil Cedex, France

To whom correspondence should be addressed: Laboratory of Neurovascular Biology, Candiolo Cancer Institute, Strada Provinciale 142 km 3,95, 10060 Candiolo, Torino, Italy. Tel.: 390119933508; Fax: 390119933524; E-mail:marco.arese@unito.it.
Both authors contributed equally to the project.

Abstract

The synaptic protein Neuroligin 1 (NLGN1), a cell adhesion molecule, is critical for the formation and consolidation of synaptic connectivity and is involved in vascular development. The mechanism through which NLGN1 acts, especially in vascular cells, is unknown. Here, we aimed at deepening our knowledge on the cellular activities and molecular pathways exploited by endothelial NLGN1 both *in vitro*and *in vivo*. We analyzed the phenotypic consequences of NLGN1 expression modulation in endothelial cells through *in vitro* angiogenesis assays and the mouse *postnatal retinal angiogenesis model*. We demonstrate that NLGN1, whereas not affecting endothelial cell proliferation or migration, modulates cell adhesion to the vessel stabilizing protein laminin through cooperation with the α6 integrin, a specific laminin receptor. Finally, we show that *in vivo*, NLGN1 and α6 integrin preferentially colocalize in the mature retinal vessels, whereas NLGN1 deletion causes an aberrant VE-cadherin, laminin and α6 integrin distribution in vessels, along with significant structural defects in the vascular tree.

Introduction

The extracellular matrix (ECM)[7] provides essential support for the growth and organization of blood vessels (1). During sprouting angiogenesis, endothelial cells (ECs) secrete matrix proteins such as vitronectin, fibronectin, and collagen I leading to the formation of a provisional ECM, which sustains ECs proliferation and migration (2). Moreover, ECM proteins coordinate or at least complement the sprouting process by modulating the differentiation of the so-called tip and stalk cells (3, 4). When the angiogenic stimulus drops, ECs arrest the migration and proliferation processes, form a lumen, and re-establish functional VE-cadherin-mediated cell-to-cell adherens junctions (5). ECs are normally quiescent although they are bound to vascular basement membrane (BM), a specialized form of ECM of mature vessels, mainly composed of laminin, collagen IV, heparan sulfate, and proteoglycans. Hence, the primary signals originating from BM inhibit proliferation and promote an environment that facilitates appropriate cell to cell adhesion. The main cellular sensors of cell-ECM adhesion are integrins, a large family of dimeric transmembrane proteins displaying different affinities for the ECM components.

Neuroligins (NLGNs) are neuronal proteins involved in the modulation of synaptic transmission (6). Recently, we have demonstrated that they have a function in vascular biology (7), and that a mature ECM has a pivotal role in vascular development and angiogenesis (7–9). In particular, the use of a zebrafish model combined with the knockdown of multiple genes (8) suggested that ECM is a critical component of NLGN signaling during vascular development, allowing

the organization of ECM-immobilized vascular endothelial growth factor-A (VEGFA) gradients necessary for capillary networking (10) (11). Moreover, in ECs the cellular processes and molecular pathways in which NLGNs are involved remained unknown. In this article we show that NLGN1 promotes cell adhesion selectively on the BM protein laminin, and induces *in vitro* cord formation of ECs plated on BM by cooperating with α6 integrin, an integrin subunit that forms widely distributed endothelial laminin receptors (12). Furthermore, *in vivo*, NLGN1 deletion causes important organizational/morphological defects in the vascular tree of the developing mouse retina as well as in the structure of single vessels. This is demonstrated by deranged cell to cell junctions and disturbed laminin distribution, especially in the areas where NLGN1 and α6 co-localize. To our knowledge, this is the first report of a neuronal synaptic protein that functionally interacts with an integrin to modulate cell to ECM adhesion in the vascular system.
Previous SectionNext Section

EXPERIMENTAL PROCEDURES

Animals

Mice lacking NLGN1 (Nlgn1^{tm1}Bros/J, Jackson Laboratory), previously described in Ref. 13, were maintained on a mixed C57BL/6 × 129 background (designated B6; 129) in the animal facility of the Institute for Cancer Research (IRCC) under standard housing conditions. Mice were sacrificed at postnatal (P) 5, and retinas were isolated for analysis. PCR amplification was used for the genotype characterization using the forward common primer (5'-GTGAGCTGAATCTTATGGTTAGATGGG-3'), the wild type reverse primer (5'-CGAGAGTCAGGTAAATTGAACACCAC-3'), and the mutant reverse primer (5'-GAGCGCGCGCGGCGGAGTTGTTGAC-3'). All animal experiments were performed in compliance with guidelines governing the care of laboratory mice of the University of Torino Committee on Animal Research.

Antibodies, Reagents, and DNA Constructs

Antibodies

Rat monoclonal function-blocking antibody against α6 integrin (Clone number GOH3, MAB 13501), anti-Dll4 (AF 1389), and VE-cadherin (AF1002) antibodies were obtained from R&D Systems. Mouse monoclonal antibody 4F9 against NLGN1 and NLGN2, and mouse monoclonal antibody 4C12 against human NLGN1 were obtained from Synaptic Systems, whereas the rabbit anti-pan-NLGNs antibody L067 (rabbit immunization with PHPHPHSHSTTRV peptide) was obtained from New England Peptide. The mouse anti-HA (sc-7392) and rabbit polyclonal anti-NLGN1 (H45, sc-50393) antibodies were purchased from Santa Cruz Biotechnology. Isolectin B4 FITC-conjugated from *Bandeiraea simplicifolia* was purchased from Sigma. The anti-glial fibrillary acid protein (GFAP) antibody was from Dako. The pan-rabbit anti-laminin (Ab2034), anti-collagen IV, anti-α3 integrin, blocking antibody (clone P1B5, MAB1952Z), and the rabbit monoclonal anti-β1 integrin (04-1109) antibodies were from Millipore. The rabbit anti-VEGF receptor 2 (VEGFR2, 2479L) antibody was purchased from Cell Signaling. The mouse anti-β4 integrin (450-11) antibody was produced as described in Ref. 14.

Reagents

The ECMs laminin, collagen I, fibronectin, vitronectin, and collagen IV were from Sigma; Lipofectamine 2000, Oligofectamine, and the Alexa Fluor conjugate were purchased from Invitrogen. Small interference RNAs (siRNAs) on-Target were obtained from Dharmacon Scientific.

DNA Construct

The NLGN1 construct (*Mus musculus*) with splicing inserts A and B carrying the HA sequence at the N-terminal end in pCAG vector and NLGN2 construct (*M. musculus*) with splicing inserts A carrying the HA sequence at the N-terminal end in the pNICE vector were from Peter Scheiffele. The retroviral vector overexpressing NLGN1 was generated using as template the KIAA1070 obtained from HUGE (database of Human Unidentified Gene-Encoded Large Proteins Analyzed) cloned in the pBlueScript vector (Invitrogen), and subcloned in the final retroviral expression vector pBABE (pBABE NLGN1). The lentiviral vector pWpXL containing the human α6 integrin Myc-tagged sequence was produced as described (15).

Cell Culture

Human umbilical vein ECs and human umbilical artery ECs were extracted from umbilical cords and cultured in EGM2 medium (Clonetics, Cambrex Bio Science, Walkersville, MD). In all experiments, ECs were used between passages 2 and 5. To overcome the intrinsic biological variability of EC, all experiments were performed with a mixture of ECs from at least three different umbilical cords.

siRNA and cDNA Transient Transfection

ECs (2×10^6) were plated in 10-cm^2 dishes and transfected in Opti-MEM® I + GlutaMAX™ (Invitrogen) with 3 µg of DNA by using the Lipofectamine™ (2 mg/ml) and Plus Reagent (3 mg/ml) (Invitrogen). After 3 h at 37 °C the Opti-MEM I was replaced with EGM-2. For transient down-regulation, ECs were seeded in EGM-2 in 6-well plates (1.2×10^5 cells/well). ECs were transfected the next 2 days with 200 pmol of each ON-TARGET plus siRNAs (Dharmacon Thermo Scientific): siRNA NLGN1_A5 (CCUGUGUGGUUUACUAAUA), or siRNA NLGN1_A6 (CCUGUGUGGUUUACUAAUA) recognizing the CDS sequences of human NLGN1, siRNA_17, which recognizes the 3'-UTR of NLGN1 human sequences (CAAAUGAGAUGGACUUAAAUU), or with Non-targeting siRNA#1 (Scramble), using Oligofectamine (Invitrogen) according to the manufacturer's protocol.

Endothelial Cells Infection

The α6 integrin-Myc pWpXL lentivirus was produced as described (7). The day before the infection, ECs were seeded at concentrations of 3.5×10^4 cells/ml in a 10-cm^2 tissue culture dish. Then the cells were transduced for 24 h with α6 integrin-Myc lentiviral particles in the presence of 8 µg/ml of Polybrene (Sigma). Before starting every experiment the efficiency of cell infection was determined by FACS analysis (BD Biosciences) using rabbit polyclonal anti-Myc antibody (AbCam).

RNA Extraction, Retrotranscription, and qRT-PCR

The total RNA was extracted using TRIzol (Invitrogen) according to the manufacturer's instructions. The mRNAs obtained were treated with a DNase-free kit (Ambion and Applied Biosystem) and quantified with NanoDrop® (ND-1000 and ND-8000 8-Sapectrophotometers). The quality of RNA was checked by the Agilent 2100 bioanalyzer (Agilent Technologies, Waldbronn, Germany). First-strand cDNA was generated from 1 µg of total RNA using the High Capacity cDNA Reverse Transcription Kit (Invitrogen). The expression of human NLGNs, mouse NLGN1, and human α6 integrin was analyzed by quantitative real-time reverse transcription-PCR (qRT-PCR) using TaqMan Gene Expression Assay (human NLGN1, Hs00208784_m1; human NLGN2, Hs00325309_m1; human NLGN3, Hs00219160_m1; human NLGN4X, Hs00535592_m1; human NLGN4Y, Hs00208784_m1; *M. musculus* NLGN1 Mm02344305_m1; human ITGa6, Hs00173952, from Applied Biosystems). The mRNA levels, analyzed in triplicate, were normalized by using as housekeeping genes the human (Hs00427620_m1) or mouse (Mm00446971_m1) TATA-binding box protein. The fold-increase or decrease was determined relatively to a control after normalizing to GAPDH (internal standard) with the formula $2^{-\Delta\Delta CT}$.

Immunoprecipitation and Immunoblotting Analysis

Subconfluent ECs or mouse brains from P5 wild-type, heterozygous and NLGN1 null mice were homogenized in cold EB buffer (10 mM Tris-HCl, pH 7.5, 150 mMNaCl, 5 mM EDTA, pH 8; 10% glycerol, 1% Triton X-100, protease and phosphatase inhibitors, 50 µg/ml of pepstatin, 50 µg/ml of leupeptin, 10 µg/ml of aprotinin, 1 mM PMSF, 100 µM ZnCl2, 1 mM sodium orthovanadate, and 10 mM NaF). After centrifugation (20 min, 4 °C at 10,000 × *g*), the supernatants were quantified with BCA Protein Assay Reagent Kit (Pierce Chemical Co.). Proteins for each sample were pre-cleared by a 1-h incubation with A-Sepharose protein (Amersham Biosciences). Each sample was then incubated overnight at 4 °C with rabbit polyclonal anti-NLGNs antibody (L067) used at a final concentration of 2.5 µg/mg of protein. The immune complexes were recovered on protein A-Sepharose for 1 h and 30 min, pelleted, and washed four times with lysis buffer. The proteins were separated by 10% SDS-PAGE electrophoresis gel, transferred to polyvinylidene difluoride membrane (PVDF, Millipore), and incubated with anti-NLGN1, -2, and -3 antibody (4F9 1:1000), or with mouse monoclonal anti-

NLGN1 antibody (4C12 1:1000) or with polyclonal anti-rabbit anti-NLGN2 antibody and visualized by ECL system (Amersham Biosciences).

Adhesion Assay

ECs (10^4/well) were resuspended in 0.1 ml of EBM-2, 0.2% BSA, plated on 96-well plates (Costar, Acton, MA) coated with laminin (10 µg/ml) and left to adhere for 30 min at 37 °C. ECs were washed twice in PBS and then fixed 30 min in 8% glutaraldehyde and stained with 20% methanol, 0.1% crystal violet for 30 min. The cells were photographed with a QIcam FAST1394 digital color camera (QImaging) and counted with Image-ProPlus 6.2 software (Media Cybernetics). In the case of functional blocking the final concentration was 10 µg/ml for anti-α6 and anti-α3 antibody treatments or the control isotype.

In Vitro Cord Formation Assay

For *in vitro* cord formation basal membrane extract (BME) (Matrigel, BD Biosciences) was added to each well at a concentration of 8 mg/ml and incubated at 37 °C for 30 min to allow gel formation. ECs ($2{,}3 \times 10^4$/well) were plated onto Matrigel and incubated for 4 h at 37 °C in 5% CO_2 humidified atmosphere. Cell organization was examined (Leica Microsystem, Heerbrugg, Switzerland) and photographed. The lengths of the capillary-like structures were quantified with the imaging software winRHIZO Pro (Regent Instruments Inc.). In the case of functional blocking the final concentration was 10 µg/ml for anti-α6 and anti-α3 antibody treatments or control isotype.

Retinal Whole Mount Staining and Confocal Imaging Analysis

Mouse retina dissection and whole mount immunostaining were performed as previously described (16) with modifications. Eyes were harvested at P5 and fixed in 4% paraformaldehyde for 1 h on ice. Retinas were dissected and washed briefly with DPBS (Sigma) three times and incubated overnight at 4 °C in DPBS containing 0.5% Triton X-100 and 0.2% BSA. The retinas were rinsed briefly with DPBS containing 1% Triton X-100 and then incubated overnight at 4 °C in DPBS, 1% Triton X-100 with specific antibodies against: isolectin B4 (40 µg/ml), NLGN1 (H45; 1:25), VE-cadherin (1:50), GFAP (1:1000), anti-pan-laminin (1:50), collagen IV (1:100), anti-Dll4 (1:50), and anti-α6 integrin (1:50). The retinas were rinsed in DPBS for 2 h and then incubated for 1 h at room temperature in DPBS, 1% Triton X-100 containing the appropriate secondary antibody Alexa Fluor conjugate (1:200 Alexa, Invitrogen Molecular Probes) and stained with DAPI (1:5000) for 45 min. Retinas were then washed in DPBS for 1 h, fixed again with 4% paraformaldehyde for 30 min at room temperature, and flat-mounted onto a glass coverslip. Images were acquired using a confocal laser-scanning microscope (TCS SP2 with DM IRE2; Leica) and processed using Adobe Photoshop® and ImageJ 1.47 version. Retina images were quantified with Image-Pro Plus 6.2 software (Media Cybernetics, "colocalization highlighter" function) as follow: the immunoreactivity was calculated as the surface area of each antibody staining colocalizing with isolectin B4, normalized on total surface vascular area visualized by isolectin B4; the percentage of colocalization between α6 integrin and laminin was calculated as the fraction (%) of colocalized area between α6 integrin and laminin normalized on the total surface vascular area visualized by isolectin B4; the colocalization between NLGN1 and α6 integrin, in positive regions of interest for both Dll4 and VE-cadherin, was considered as a mean fluorescence of colocalization between two proteins in Dll4 or VE-cadherin positive staining regions of interest, traced with "polygon selection" function of Image-Pro Plus 6.2 software.

Quantification of Angiogenic Parameters in Mouse Retina

Images were analyzed using a customized version of a plugin previously described (27), developed for the ImageJ software and available at the NIH website. Briefly, fluorescence confocal images were first assembled to build full retina pictures using the MosaicJ plugin. These mosaics were segmented and analyzed as follows: low frequencies were removed using the deblurring "unsharp mask" method and noise was reduced by Gaussian convolution and dilation. Pre-treated images were then segmented using the so called "moments" threshold method (17). Holes smaller than vascular meshes were then removed and the gross trees were obtained using the skeletonize function of ImageJ. After that the pruning was performed to remove small artifactual twigs, and junctions, segments, and connecting junctions were detected. Finally, the meshes defined as areas enclosed by segments were revealed. These structures were counted and measured inside a ring of interest, delimited by two circle selections defined by the user, and finally used for

statistical analysis. The first ring was located in a range between 500 μm (the nearest radius from the optic nerve) and 800 μm far from the optic nerve and with an area coverage of 1.22 mm, whereas the second ring was located in a range between 800 and 1100 μm far from the optic nerve and including the sprouting vascular front, with an area coverage of 1.79 mm^2. The vascular radius calculated (Fig. 3*C*, *dashed circle,* ImageJ 1.47) as the distance between vascular front and the center of the optic disc was normalized on the retinal radius. For each quantification at least 5 mice/genotype were analyzed and the corresponding values were expressed relatively to the mean retinal radius.

EC Immunostaining and Signal Quantification

ECs plated on coated coverslip with gelatin, laminin (10 μg/ml), or collagen I (10 μg/ml) were fixed with 4% paraformaldehyde for 10 min at room temperature, permeabilized with either 0.2% Triton-X in PBS for 8 min at room temperature, and saturated with 1% donkey serum in PBS for 40 min at room temperature. The slides were incubated with the following primary antibodies: mouse anti-HA (1:100), rat anti-α6 GOH3 (1:50), rabbit anti-β1 integrin (1:100), mouse anti-β4 integrin (1:100), and rabbit anti-α3 integrin (1:100) in PBS, 1% donkey serum for 1 h at room temperature. Then the appropriated Alexa Fluor secondary antibodies were added in PBS, 1% donkey serum for 45 min at room temperature. Finally, the cells were stained with DAPI (1:10,000) for 10 min at room temperature and mounted with immunofluorescence mounting medium (Dako).

The confocal images were acquired using a confocal laser-scanning microscope (TCS SP2 with DM IRE2; Leica). To quantify the degree of colocalization between two proteins we calculated the Mander's coefficient by using the JACoP plugin of ImageJ (28), whereas for the colocalization of three fluorescent proteins we used the “coloc” function on Imaris software (version 6.3.1) in maximum-projected confocal image stacks.

Co-immunoprecipitation

Subconfluent ECs, infected with α6 integrin-Myc cDNA and plated for 2 h on BME (10 μg/ml, Matrigel, BD Biosciences), were homogenized in lysis buffer containing 15 mM CHAPS, 0.15 M NaCl, 2 mM EDTA, 1 mM PMSF, 1 mM $NaVO_4$, 50 mM Tris-HCl, pH 7.5, and centrifuged 15 min at 15,000 × *g.* The immunoprecipitation was performed as described above using both rabbit polyclonal anti-NLGNs antibody (L076) and mouse monoclonal anti-Myc antibodies. For the Western blotting analysis PVDF membranes were immunodecorated with mouse monoclonal anti-NLGN1 antibody (4C12, 1:1000) and rabbit polyclonal anti-Myc antibody (1:1000) and visualized by ECL system.

Statistical Analysis

Upon verification of normal distribution, statistical significance of raw data between the groups in each experiment was evaluated using the unpaired Student's *t* test or ANOVA followed by the Bonferroni post-test. Results are expressed as mean ± S.E. when derived from averaged experiments, or mean ± S.D. when derived from several data points of one experiment. *n* represents the number of individual experiments. The asterisks (*, **, and ***) in figure panels refer to statistical probabilities (*p*) of <0.05, <0.01, and <0.001, respectively.

Previous SectionNext Section

RESULTS

NLGN1 Modulates in Vitro EC Cord Formation and Adhesion to Laminin

By virtue of the functional differences between members of the NLGN family at synapse, we began by screening the expression of the different NLGN isoforms in vascular tissues and cells. Fig. 1, *A* and *B*, shows that the most expressed isoforms of NLGN in ECs were NLGN1 and -2. These two isoforms were chosen as targets and their role in endothelial functions related to angiogenesis was investigated by gain and loss of function approaches (validated in Fig. 1, *C* and *D*).

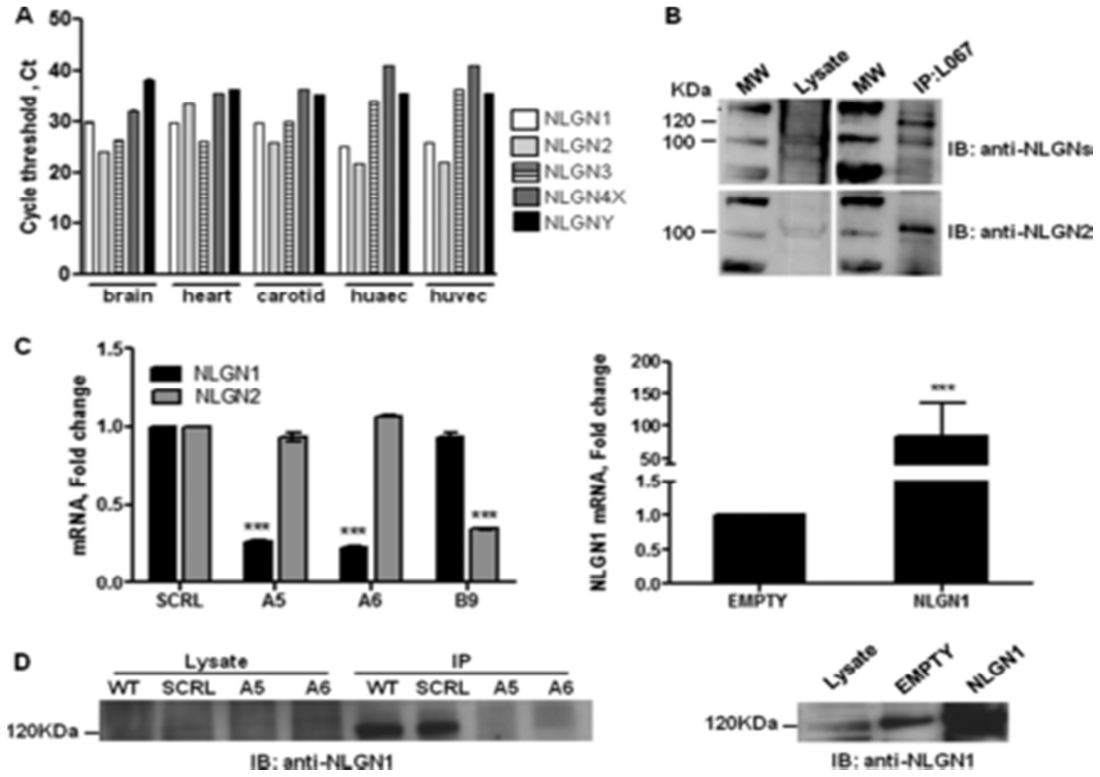

FIGURE 1.

Screening of NLGN isoforms expression and validation of NLGN silencing and overexpression efficiency in ECs. *A,* NLGN1, -2, -3, -4X, and -4Y expression is presented for primary cells (human umbilical vein and human umbilical artery ECs) and organs (brain, heart, and carotid). NLGN mRNA levels were assessed by qRT-PCR and the graph shows the single threshold cycle (Ct), which is inversely correlated to the expression level. The data revealed NLGN1 and NLGN2 as the most expressed isoforms in the ECs. Values are mean ± S.E. of three independent experiments. B, immunoprecipitation assay was performed in ECs using an anti-pan-NLGNs (L067) antibody and immunoblotting was conducted with a monoclonal antibody (4F9) able to recognize NLGN1 and NLGN2 isoforms (top panel). The membrane was then stripped and incubated with a polyclonal antibody recognizing only NLGN2 (bottom panel). The 120- and 100-kDa bands detectable in ECs correspond to NLGN1 and NLGN2, respectively. The images shown are representative of 1 of 3 reproducible experiments. C, left panel:qRT-PCR of NLGN1 and NLGN2 expression level on ECs transfected with control siRNA (SCRL), with two independent specific siRNA sequences targeting NLGN1 (A5 and A6) or with one specific siRNA sequence targeting NLGN2 (B9). Fold-change is calculated with respect to cells transfected with siRNA SCRL and values are expressed as mean ± S.E. (n= 3 independent experiments). One-way ANOVA with Bonferroni test: ***, $p < 0.001$. Right panel: qRT-PCR of NLGN1 expression level on ECs infected with the retroviral vector pBABE EMPTY (EMPTY) or containing the human cDNA sequence of NLGN1 (NLGN1). Results are expressed as fold-change relative to pBABE EMPTY. Values are mean ± S.E. (n = 3 independent experiments). One-way ANOVA with Bonferroni test: ***, $p< 0.001$. D, immunoprecipitation assay performed using the pan-NLGNs antibody (L067) in ECs transfected with control siRNA (SCRL) or NLGN1 siRNAs (A5 and A6) (left panel) or infected with pBABE EMPTY (EMPTY) or pBABE NLGN1 (NLGN1) retroviral vector (right panel). Immunoblottings (IB) were carried out using the monoclonal antibody 4C12, which specifically recognizes NLGN1. Images shown are representative of 1 of 3 experiments.

Although down-regulation of NLGN1 or -2 did not affect cell migration, haptotaxis, and cell proliferation (data not shown), the silencing of NLGN1 modified the spontaneous cord formation of ECs seeded on BME. As shown in Fig. 2*A* (*upper panel*) NLGN1-silenced ECs formed a significantly less structured network compared with the control and NLGN2-silenced ECs. To further verify the specific involvement of NLGN1 in vascular organization, we analyzed ECs overexpressing NLGN1 and demonstrated that these cells formed a more complex network related to control cells (Fig. 2*A, lower panel*).

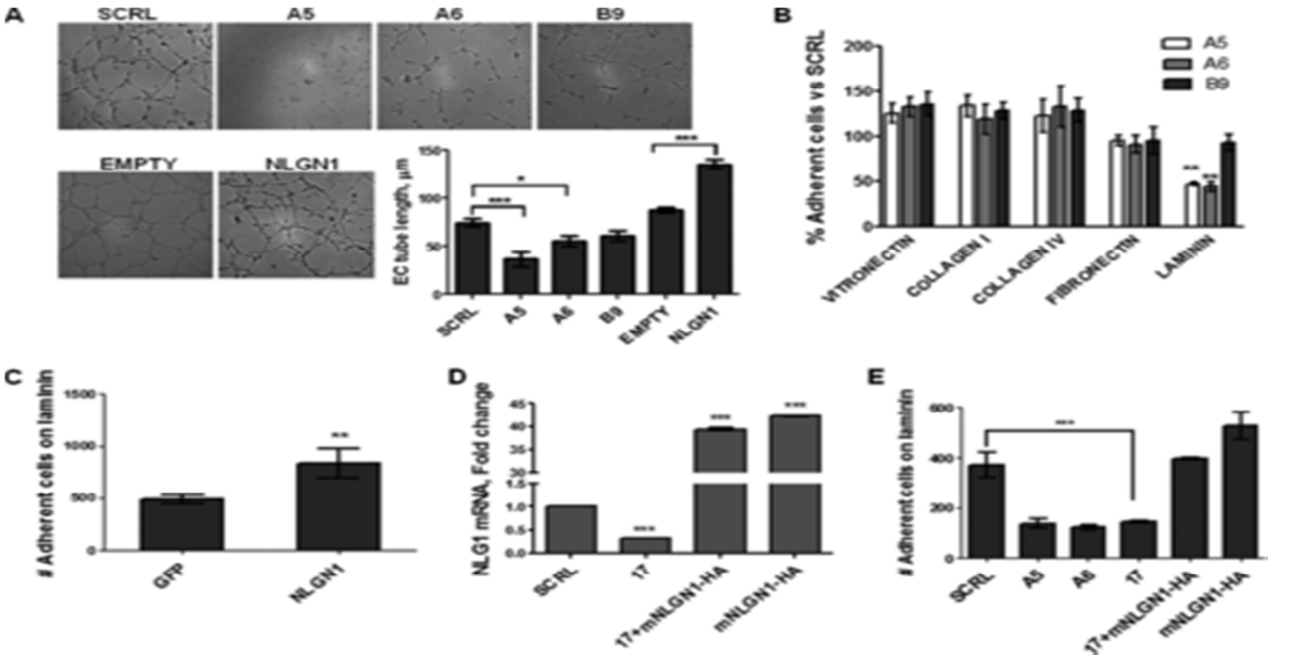

FIGURE 2.
NLGN1 is specifically involved in EC morphogenesis and adhesion to laminin. Cord formation (*A*) and adhesion (*B*,*C*, and *E*) assays were performed on ECs transfected with control siRNAs (*SCRL*) or siRNAs targeting either NLGN1 (*A5*, *A6*, and *17*) or NLGN2 (*B9*), or ECs overexpressing either NLGN1 (HA-tagged mouse NLGN1, mNLGN1-HA, or retroviral vector pBABE NLGN1, *NLGN1*) or control pBABE vectors (*EMPTY* or *GFP*). *A*, ECs were seeded on 48-well plates coated with BME (8 mg/ml) and photographed after 4 h to evaluate cord formation. Images are representative of 1 of 3 reproducible experiments. The graph displays the mean EC tube length, quantified through WinRHIZO Pro, of three representative experiments ± S.E. One-way ANOVA with Bonferroni test: *, $p < 0.05$; ***, $p < 0.001$. *B,* ECs were allowed to adhere on 96-well plates coated with fibronectin (1 µg/ml), collagen I (10 µg/ml), collagen IV (2 µg/ml), vitronectin (1 µg/ml), or laminin (10 µg/ml) for 30 min at 37 °C. After crystal violet staining, cells were counted employing Image ProPlus, to evaluate the adhesion rate. Results are expressed as the percentage of adherent cells relative to non-targeting siRNA. Values are expressed as mean ± S.D. of one representative experiment (of two) performed in triplicate. One-way ANOVA with Bonferroni test: **, $p < 0.01$. *C,*adhesion assay was performed on ECs transfected as indicated and plated on laminin (10 µg/ml), as in *panel E.* Values are mean ± S.E. of three independent experiments. Unpaired Student's *t* test, two tailed: **, $p < 0.01$. *D,* NLGN1 mRNA levels, evaluated by qRT-PCR, in ECs transfected with siRNA NLGN1_17 (which targets the 3'-UTR sequence of human NLGN1) 24 h before transfection of mouse HA-tagged NLGN1 cDNA. The graph highlights that siRNA NLGN1_17 does not affect the overexpression of the mouse HA-tagged NLGN1 mRNA. Results are expressed as fold-change relative to control siRNA (*SCRL*). Values are mean ± S.E. of three independent experiments, ***, $p < 0.001$. *E*, ECs were transfected as indicated and the adhesion assay (as in *panel B*) was performed on laminin. Values are expressed as mean ± S.D. of a representative experiment of three, performed in triplicate. One-way ANOVA with Bonferroni test: ***, $p < 0.001$.

Because the process of cell adhesion to different ECM proteins is an important step in endothelial morphogenesis, we tested the adhesion capability of NLGN1 or -2 down-regulated ECs. The endothelial cells were plated on several components of provisional and mature ECM, *i.e.* fibronectin, collagen I, collagen IV, vitronectin, or laminin (Fig. 2*B*). The screening indicated that NLGN1 (but not NLGN2)-silenced cells displayed a reduced adhesion on laminin but not on any of the other matrix proteins, when compared with control cells. We then verified that NLGN1 overexpression in EC enhanced cell adhesion to laminin (Fig. 2*C*). To confirm the specificity of the NLGN1-induced phenotype in siRNA-treated cells, we performed a “rescue” experiment. The overexpression of the mouse HA-NLGN1, which is not targeted by the human 3'-UTR targeting siRNA (siRNA17, Fig. 2*D*), fully rescued the EC adhesion to laminin (Fig. 2*E*). These results demonstrated that NLGN1 is specifically involved in the adhesion of ECs to the ECM protein laminin.

NLGN1 Modulates in Vivo Angiogenesis in the Mouse Retina

Given the role of NLGN1 in zebrafish vascular development (8) and in endothelial cord formation *in vitro*, we investigated postnatal retinal angiogenesis in P5 WT and NLGN1 null mice. In WT retinas, NLGN1 (Fig. 3*A*, *upper panel*, *red*) was expressed in vessels in most of the region marked by isolectin B4 (Fig. 3*A*, *upper panel*, *green*), whereas it was not detectable in NLGN1 null mice (Fig. 3*A*, *lower panel*, *red*).

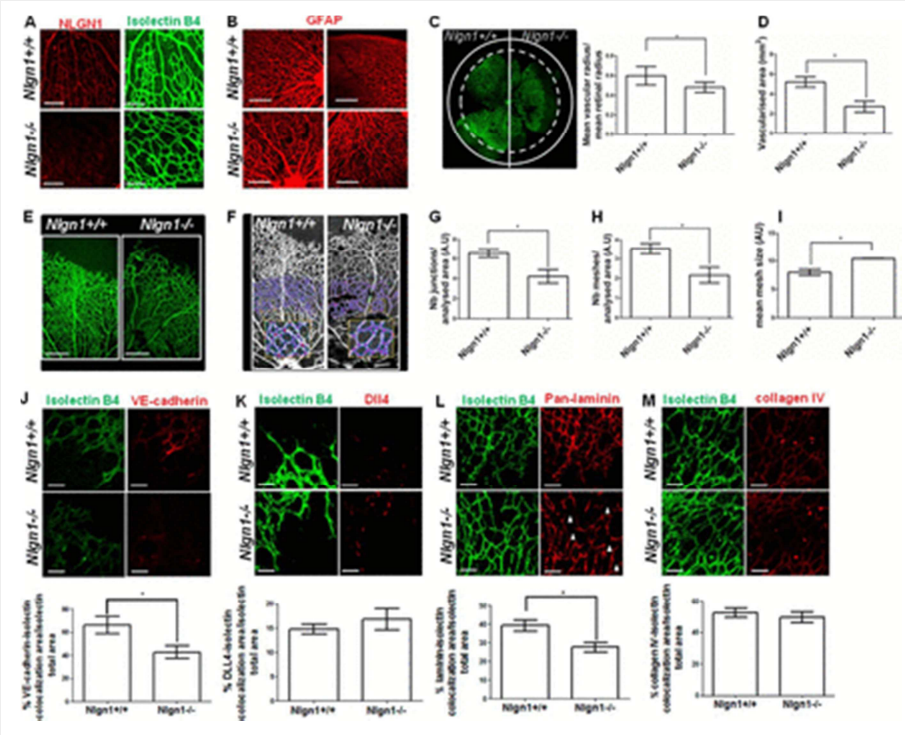

FIGURE 3.

NLGN1 null mice display an abnormal retinal angiogenesis.*A,* P5 mouse retina of WT ($Nlgn1^{+/+}$) and NLGN1 null ($Nlgn1^{-/-}$) mice were immunostained with isolectin B4 to visualize the retinal vascular vessels (*green*) and with the anti-NLGN1 antibody (clone H-45, *red*), which revealed no specific signal in NLGN1 null mice (*bottom panel*) compared with WT mice (*top panel*). *Scale bar*: 100 μm, $n = 6$ mice for each genotype. *B*, P5 retinas of both WT ($Nlgn1^{+/+}$) and NLGN1 null ($Nlgn1^{-/-}$) mice were immunostained with the anti-GFAP antibody to visualize the astrocytes. Images highlight the correct organization of astrocytes in NLGN1 null mice. $n = 12$ retinas for each genotype. *Scale bar*: 200 μm. *C-I*, evaluation of angiogenic parameters on P5 retinas of both WT and NLGN1 null mice ($n = 15$ retinas for each group) immunostained with the vascular marker isolectin B4. *C,* the confocal image highlights the differences in terms of vascular radius (*C*, *left panel*), quantified through the dashed circle tool of ImageJ 1.47, and the vascular area (*D*), evaluated through the Angiogenesis Analyzer plug-in for ImageJ. *E* and *F,* the images illustrate the altered vascular pattern of NLGN1 null mice (*E*) and the snapshot exhibiting the obtained model (*F*) used for the analysis of the number of junctions (*G*), the number of meshes (*H*), and the size of meshes (*I*). These parameters were calculated with the Angiogenesis Analyzer plug-in for ImageJ, in a circular area between 500 and 800 μm from the optic nerve (covered area of 1.22 mm^2) representing a sample of a mature region of the network that excludes the growing front of the plexus. Values are expressed as mean ± S.E. ($n = 3$ independent experiments). Unpaired Student's *t* test, two-tailed resulted in: *C,* *, $p = 0{,}033$; *D,* *, $p = 0.012$;*G,* *, $p = 0.026$; *H,* *, $p = 0.030$; *I,* *, $p = 0.011$. *Scale bars*: *E*, 200 μm.*J-M*, confocal microscopy analysis of vascular markers on P5 retinas of both WT ($Nlgn1^{+/+}$) and NLGN1 null mice ($Nlgn1^{-/-}$) ($n = 12$ retinas for each group). Retinas were immunostained with isolectin B4 in combination with VE-cadherin (*J*), Dll4 (*K*), pan-laminin (*L*), or collagen IV (*M*). The percentage of colocalization was calculated with Image-Pro Plus 6.2 software as the

surface area of each antibody staining, colocalizing with isolectin B4, normalized on the total surface vascular area. Values are expressed as mean ± S.E. (*n* = 3 independent experiments). Unpaired Student's *t* test, two-tailed results were: *J,* *, *p*= 0.047; *K, p* = 0.431; *L,* *, *p* = 0.020; *M,* *, *p* = 0.062. *Scale bars* for *J–M*, 50 μm.

Although the GFAP-positive astrocytic network, which is known to provide guidance to the growing vessels (18), displayed no morphological difference between WT and NLGN1 null mice retinas (Fig. 3*B*), significant anomalies were identified in the retinal vascular tree of NLGN1 null mice by staining with isolectin B4 (Fig. 3, *C–I*). The defects included a shorter vascular radius (Fig. 3*C*), a reduced total vascularized area (Fig. 3*D*), and a decrease in the complexity of the vascular network (Fig. 3, *E* and *F*). This last feature consisted in a reduced number of junctions (Fig. 3*G*) and meshes (Fig. 3*H*) as well as in an increase in the size of the meshes (Fig. 3*I*). Interestingly, the reduction in the complexity of the vascular network was especially evident in the mature region of the retinal plexus, and measurements were made in a specific circular area of the plexus as illustrated by the schematization in Fig. 3*F*. The involvement of NLGN1 in the maturation/stabilization of the vessels was in agreement with the fact that NLGN1 did not modulate migration/haptotaxis or proliferation of ECs. Moreover, NLGN1 was involved in EC adhesion to laminin, which is a component of mature ECM, but not to "angiogenesis promoting" matrix proteins such as collagen I, fibronectin, and vitronectin (2). Indeed, NLGN1 deletion caused a significant loss of the presence of VE-cadherin at cell-to-cell junctions (Fig. 3*J*), whereas Dll4 expression and distribution, an indicator of sprouting vasculature (19), remained unchanged between WT and NLGN1 null mice (Fig. 3*K*). Moreover, prompted by our *in vitro*data we analyzed laminin and collagen IV localization in WT and NLGN1 null mice. Intriguingly, we found that the distribution of laminin (Fig. 3*L*), but not that of collagen IV (Fig. 3*M*), was affected in the retinal vascular plexus of NLGN1 null mice. In particular, laminin appeared delocalized from vessels in many sites throughout the network. These data indicated a role for NLGN1 in the formation of EC junctions and in the correct patterning of laminin in the BM. Ultimately, this can lead to an alteration in the morphology of the vascular tree and a reduction of the vascularized area.

NLGN1 Role in Adhesion and Cord Formation Depends on a Functional α6 Integrin

Because the integrin receptors for laminins in ECs are the α6β1 (15), α6β4 (12), and α3β1 (20) dimers, our first approach was to use anti-α6 or anti-α3 integrin-blocking antibody to treat NLGN1 overexpressing ECs in the adhesion and cord formation assays. We found that functional blocking of integrin α6 inhibited the NLGN1-induced cord formation on BME (Fig. 4*A*). The anti-α3 integrin antibody slightly inhibited cord formation of ECs carrying the empty vector, but it was fully ineffective on ECs overexpressing NLGN1. Similarly, the anti-α6 antibody (GOH3) totally abolished the cell adhesion induced by NLGN1 on laminin, whereas the anti-α3 antibody was ineffective (Fig. 4*B*).

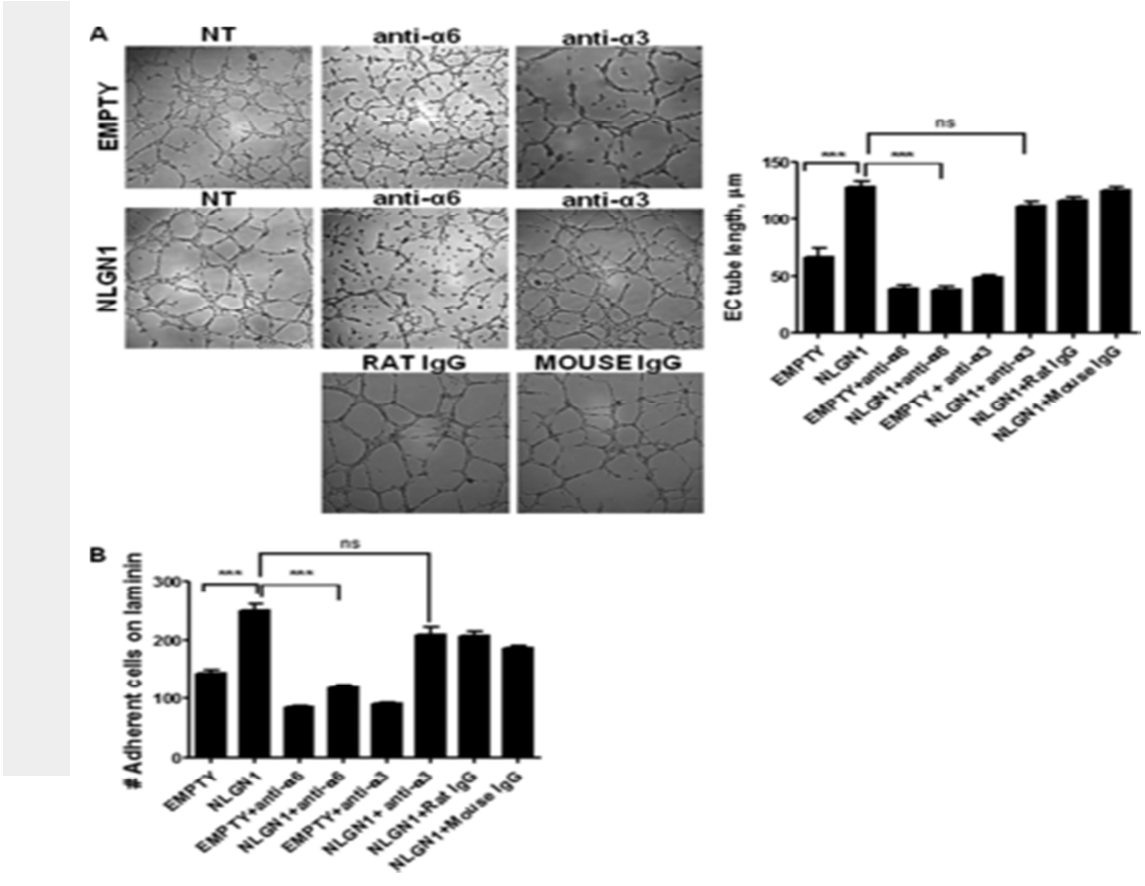

FIGURE 4.

NLGN1 modulates adhesion and cord formation in cooperation with the α6 integrin in ECs. *A,* ECs overexpressing retroviral vector pBABE, EMPTY, or containing NLGN1 cDNA (pBABE NLGN1) were seeded on 48-well plates coated with BME (8 mg/ml) and treated 4 h with blocking antibody for α6 integrin (*GOH3*), α3 integrin, or non-related rat or mouse IgGs. Tube length was quantified through WinRHIZO Pro and is represented in the histograms. Images and graphs shown are representative of 1 of 3 reproducible experiments, each in triplicate. Data are expressed as mean ± S.D. One-way ANOVA with Bonferroni test: ***, $p < 0.001$ for pBABE EMPTY *versus* pBABE-NLGN1 and for pBABE-NLGN1 *versus* pBABE-NLGN1 + anti-α6 (GOH3). *B*, the adhesion assay was performed by plating cells on 96-well plates coated with laminin (10 μg/ml). Cells infected with the retroviral vector pBABE, EMPTY, or containing NLGN1 cDNA (*NLGN1*) were treated with the α6 integrin blocking antibody (*GOH3*), the α3 integrin blocking antibody or non-related rat or mouse IgGs and allowed to adhere at 37 °C for 30 min. Data show that the GOH3 antibody completely abolished the NLGN1-induced adhesion on laminin. Data are expressed as mean ± S.D. of a representative experiment (of three) performed in triplicate. One-way ANOVA with Bonferroni test: ***, $p < 0.001$ for pBABE-EMPTY*versus* pBABE-NLGN1 and pBABE-NLGN1 *versus* pBABE-NLGN1 + anti-α6 (GOH3). *NS,* not significant.

NLGN1 Modulates the α6 Integrin-laminin Distribution in Retinal Vessels

We then investigated NLGN1 and α6 integrin cooperation and if their role in controlling adhesion and cord formation *in vitro* was matrix dependent.

We performed an immunofluorescence assay in ECs plated on laminin or collagen I. The HA-tagged NLGN1-transfected ECs were probed with the anti-HA and GOH3 antibodies. As shown in Fig. 5*A*, HA-NLGN1 and α6 integrin co-localized at the cell membrane of ECs plated on laminin significantly more than in ECs plated on collagen I.

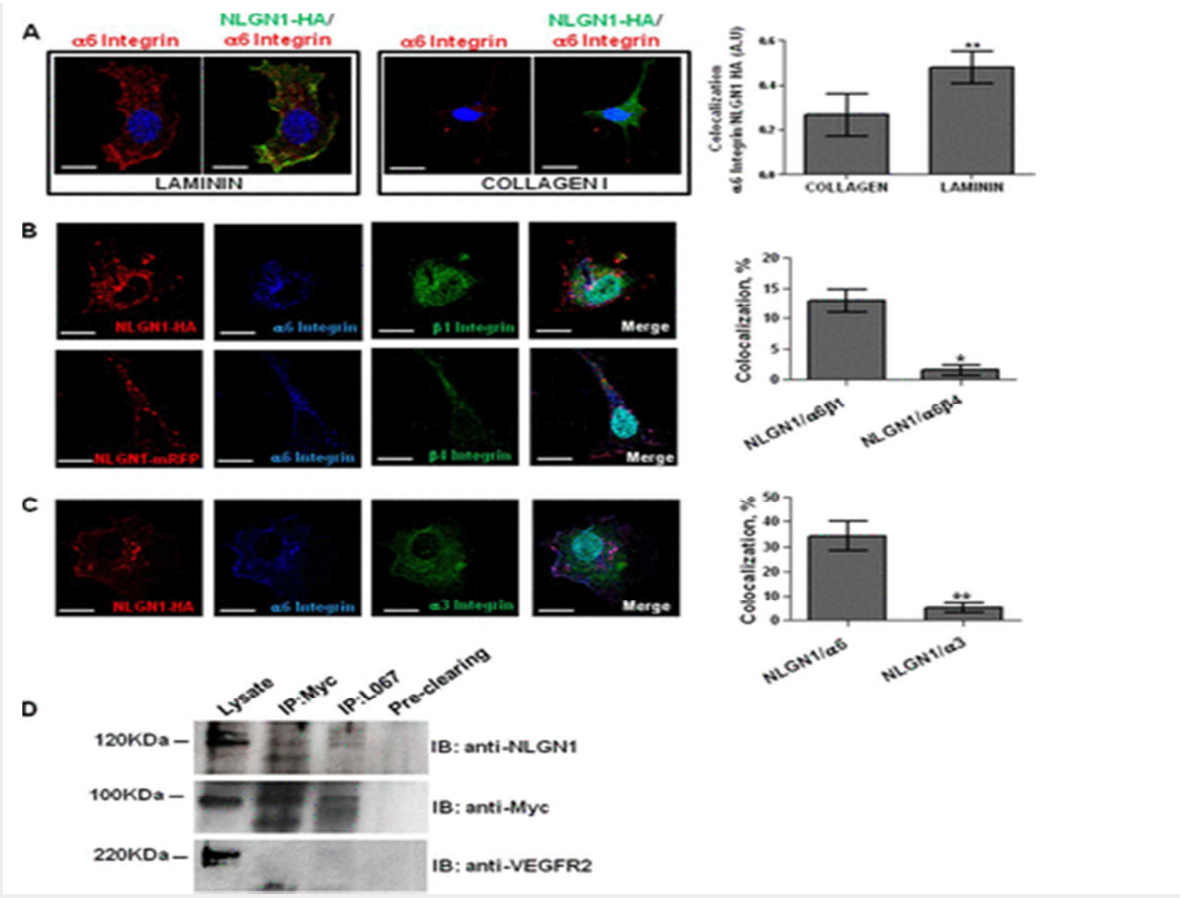

FIGURE 5.

NLGN1 and α6 integrin: colocalization and co-immunoprecipitation in ECs.*A–C*, confocal microscopy analysis performed on ECs transfected with mouse NLGN1-HA (mNLGN1-HA) or NLGN1-mRFP and plated 2 h on laminin (10 μg/ml) or

collagen I (10 µg/ml). *A*, NLGN1 and α6 integrin colocalize on laminin. ECs were immunostained with anti-HA (*green*) and anti-α6 integrin (*red*) antibodies. The images are representative of 1 of 3 reproducible experiments. *Scale bar*: 10 µm. The graph shows the colocalization index ± S.E. (*n* = 3, total cells analyzed *n* = 10), unpaired Student's *t* test, two-tailed (**, *p* = 0.0011) for laminin *versus* collagen I. *B,* NLGN1 and α6β1 integrin co-localize in ECs plated on laminin. ECs were immunostained with anti-HA (*red*), anti-α6 integrin (*blue*) in combination with anti-β1 integrin (*green*, *upper panel*) or anti-β4 integrin (*green*, *lower panel*) antibodies. The images are representative of 1 of 5 reproducible experiments. *Scale bar*: 10 µm. The graph shows the percentage of colocalization between NLGN1/α6/β1 integrin and NLGN1/α6/β4 integrin ± S.E. (*n* = 3, total cells analyzed *n* = 10), unpaired Student's *t* test, two-tailed (*, *p* = 0.023). *C,* NLGN1 and α3 integrin do not colocalize on laminin. ECs were immunostained with anti-HA (*red*), anti-α6 integrin (*blue*), and anti-α3 integrin (*green*) antibodies. The images are representative of 1 of 3 reproducible experiments. *Scale bar*: 10 µm. The graph shows the percentage of co-localization between NLGN1/α6 integrin and NLGN1/α3 integrin ± S.E. (*n* = 3, total cells analyzed *n* = 10), unpaired Student's *t* test, two-tailed (**, *p* = 0.008). *D,* co-immunoprecipitation assays were performed on ECs infected with a lentiviral vector containing the Myc-tagged α6 integrin cDNA and plated on BME (10 µg/ml) for 2 h. Proteins were immunoprecipitated either with the rabbit anti-pan-NLGNs (L067) or the mouse anti-Myc antibodies. Immunoblottings (*IB*) were carried out using the monoclonal antibody (4C12) specifically recognizing NLGN1 (band detected at 120 kDa), the rabbit anti-Myc antibody recognizing α6 integrin (band detected at 100 kDa) or, as negative control, the rabbit anti-VEGF receptor 2 antibodies (band detected at 220 kDa). The images are representative of 1 of 3 reproducible experiments.

Although it is known that the β4 integrin forms a laminin receptor with α6 in a small subset of ECs (12), we wanted to clarify which β subunit (β1 or β4) of the integrin α6 heterodimer was functionally involved with NLGN1 in ECs. Confocal imaging analyses performed in ECs plated on laminin showed a significant colocalization between NLGN1 and α6β1 dimer rather than with α6β4 dimer (Fig. 5*B*). Accordingly to the functional results cited above, we did not observe any significant colocalization of NLGN1 with α3 integrin (Fig. 5*C*). Hence, the α6β1 dimer appeared as the main laminin receptor that cooperates with NLGN1 in ECs.

As an indication that NLGN1 and α6 could be part of the same molecular complex we transduced ECs with lentivirus carrying a Myc-tagged integrin α6 protein. Then, we plated these cells on BME to perform a co-immunoprecipitation experiment. Each of the 2 proteins was immunoprecipitated and the resulting precipitate was immunoblotted with the antibody against its respective partner. In these conditions endogenous endothelial NLGN1 and exogenous Myc-α6 integrin co-precipitated (Fig. 5*D*), whereas VEGFR2 (KDR), which is well expressed in ECs, did not.

To characterize the respective localization of NLGN1 and α6 integrin *in vivo*, we analyzed the colocalization in the retinal vascular plexus. We found that in P5 WT retinas, NLGN1 and α6 integrin colocalized (*arrowheads* in Fig. 6*A*) in retinal vessels. Interestingly, we found that NLGN1/α6 integrin colocalization was higher in areas of mature vessels marked by the presence of VE-cadherin at cell-to-cell junctions, rather than at the growing front/tip cells, as marked by Dll4 (Fig. 6*B*). Importantly, the morphological defects in NLGN1 null mice were more evident in the mature vessels (Fig. 3*F*).

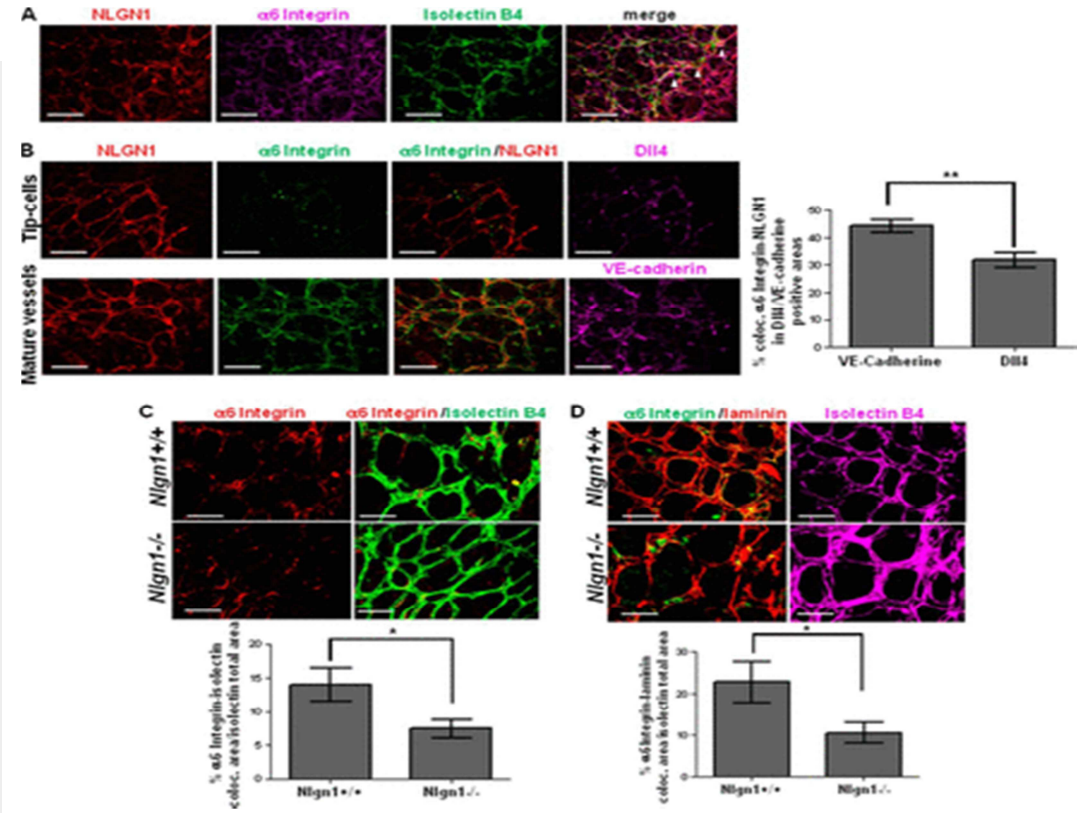

FIGURE 6.

NLGN1, α6 integrin and laminin colocalize *in vivo* in the retinal vascular tree. *A*, *in vivo* co-localization of NLGN1 and α6 integrin. P5 retinas of NLGN1 WT mice were immunostained with anti-NLGN1 (*red*), anti-α6 integrin (*magenta*) antibodies, and isolectin B4 (*green*). The*arrowheads* highlight the colocalization areas between NLGN1/α6 integrin/retinal vessels, resulting in white spots (n = 6 retinas for each group). *B,*NLGN1/α6 integrin colocalization in the mature region of retinal vessels. Immunofluorescence assays were performed on NLGN1 WT P5 retinas using either the anti-Dll4 antibody to stain "tip cells" (*top panels magenta*, pseudocolored) or the anti-VE-cadherin antibody to stain "mature vessels" (*bottom panels*, *magenta*, pseudocolored), in combination with the anti-NLGN1 (*red*, pseudocolored) and the anti-α6 integrin antibodies (*green*, pseudocolored). Data are expressed as the percentage of colocalized NLGN1 and α6 integrin signals in Dll4 or VE-cadherin positive areas ± S.E. (n = 3 retinas for each genotype), unpaired Student's t test, two-tailed (**, p = 0.0015). The graph shows that NLGN1 and α6 integrin colocalize preferentially in the VE-cadherin positive vessels. *C*, immunofluorescence stainings were performed on both WT and NLGN1 null mice P5 retinas using the isolectin B4 (*green*) and the anti-α6 integrin (*red*) antibodies. The graph shows the percentage of colocalization calculated as the surface area of α6 integrin staining colocalized with isolectin B4, normalized on the total surface vascular area. Values are expressed as mean ± S.E. (n = 3 retinas for each genotype), unpaired Student's t test, two-tailed (*, p = 0.035). Data revealed a higher expression of α6 integrin in blood vessels of WT compared with NLGN1 null mice. *D,* immunofluorescence stainings were performed on both WT and NLGN1 null mice P5 retinas using isolectin B4 (*magenta*, pseudocolored), anti-α6 integrin (*green*, pseudocolored), and anti-laminin (*red*) antibodies. The graph shows the percentage of co-localization of α6 integrin and laminin, normalized on total surface vascular area. Values are expressed as mean ± S.E. (n = 3 retinas for each genotype), unpaired Student's t test, two-tailed (*, p = 0.039). Data revealed that, in the presence of NLGN1, α6 integrin is significantly more co-localized with laminin. *Scale bars* in *A–D*, 50 μm.

Based on these data, we evaluated if the NLGN1 loss would induce a redistribution of α6 integrin localization, by quantifying the percentage of α6 integrin localized in vessels in WT and NLGN1 null retinas. In accordance with the abnormal distribution of laminin in the vascular BM of NLGN1 null mice (Fig. 3*L*,*arrowheads*), α6 integrin showed a decreased percentage of colocalization with the endothelial marker isolectin B4 in NLGN1 null mice compared with WT (Fig. 6*C*). To evaluate if, in the absence of NLGN1, α6 integrin was also delocalized from its ligand, we analyzed the co-

distribution of vascular laminin and α6 integrin. The analysis revealed that the laminin/α6 integrin colocalization in NLGN1 null mice was about 50% lower than in normal mice (Fig. 6*D*). These data imply that NLGN1 modulates the interaction between α6 integrin and laminin and contributes to the formation of a normally structured basal lamina.

Previous SectionNext Section

DISCUSSION

In this article we have deepened our knowledge on the cellular activities and molecular pathways of endothelial NLGN1. In particular we have demonstrated that NLGN1 (*a*) modulates vascular morphogenesis *in vitro* and in the mouse retina, (*b*) modulates cell adhesion on the extracellular matrix protein laminin but not on collagen I/IV, fibronectin, or vitronectin, and (*c*) cooperates with α6 integrin in modulating cell adhesion to laminin. Moreover, *in vivo*, NLGN1 and α6 integrin preferentially colocalize in the stable/mature retinal vessel, whereas the loss of NLGN1 causes significant disturbances to both VE-cadherin and α6 integrin/laminin localization.

The link between NLNG1 function and ECM that we describe here is in accordance with our previous observations in zebrafish. In that case, we showed that NLGN1 loss causes developmental defects in the caudal plexus and subintestinal vessels of the zebrafish embryo, through a synergistic activity with both the ECM binding isoforms of VEGFA and the ECM-maturation promoting enzyme heparan sulfate 6-*O*-sulfotransferase 2 (8) (9).

Our experiments show that the ablation of NLGN1 induces retinal vascular defects characterized by a reduction of the total vascularized area as well as a shorter vascular radius, suggesting a possible role of NLGN1 in sprouting angiogenesis. However, further analysis revealed that these defects may be a consequence of impaired vessel maturation. In particular we detect an altered pattern of the network meshes that becomes more evident close to the optic nerve, combined with a significant loss of the presence of VE-cadherin at the cell-to-cell junctions and a loss of laminin-blood vessel contacts. Moreover, NLGN1 does not affect EC proliferation or migration *in vitro* or the number of Dll4-positive tip cells *in vivo*. Finally, NLGN1 cooperates with α6 integrin, which is involved in vessel stabilization (1). The role of α6 integrin in angiogenesis appears to be context dependent. Functional blockade of α6 integrin inhibits the early phases of angiogenesis (15). However, complete genetic ablation of α6 integrin leads to perinatal death of mice without evidence of developmental angiogenesis defects (21), whereas endothelial-specific elimination of this integrin increases tumor angiogenesis and growth in a xenograft model (22). Here, we show that in cooperation with NLGN1 α6 integrin induces vessel stabilization in one of the most useful models for analyzing the molecular and cellular mechanisms regulating angiogenesis. The *in vivo* influence of NLGN1 on vessel stabilization is further supported by the *in vitro* data, which demonstrate that ECs adhesion to purified laminin is impaired upon NLGN1 loss.

Furthermore, laminin found in the vascular basal lamina is a mixture of several protein isoforms (23). The laminin protein that we used for the adhesion assays (Fig. 1) is not a specific isoform but is extracted from BM; similarly the antibody that we used (Fig. 2) is raised against a mixture of laminins extracted from BM. Hence, we cannot argue about which laminin isoform is involved in the NLGN1/α6 integrin activity. In this context, α6 integrin has been shown to induce Dll4 expression upon laminin-111 (24) and laminin 511-411 (4) engagement. Given the absence of an effect on Dll4 expression *in vivo* upon NLGN1 loss, we suggest that by cooperating with NLGN1, α6 integrin activity shifts toward vessel stabilization.

Some final observations can be made about the implications and parallels that our data may have in neurobiology. First, we show that NLGN2 does not mediate the same cellular activities of NLGN1 in ECs. This is a very interesting similarity with the selective and differential NLGN1 and NLGN2 activities at excitatory and inhibitory synapses, respectively, and perhaps depends on the recruitment of alternative downstream partners in ECs as in neurons (6). Ongoing experiments in our laboratory are dedicated to understanding the role of NLGN2 in ECs. Second, it is possible that the role of NLGN1 in cell adhesion to laminin extends to the central nervous system, where laminin is also present. On one hand, this is conceptually supported by the fact that Neurexin, the natural pre-synaptic partner of NLGN1 contains LNS domains (25), which are present in laminin (26).

In conclusion, our article brings novel data into the vascular role of NLGN1 and introduces some novel working hypotheses on its activity in the nervous system. In particular it would be interesting to analyze if the ECM, as in vascular development, also plays a role in neural plasticity.

Footnotes

This work was supported by Associazione Italiana per la Ricerca sul Cancro (AIRC) investigator Grants IG 11503 (to M. A.), 10133 (to F. B.), AIRC 5 × 1000 (code 12182), Fondazione Umberto Veronesi, Young Investigator Grant 2014 (to M. A.), Regione Piemonte: Ricerca Sanitaria Finalizzata, 2008, Converging Technologies Program grant "Photonic Biosensors for Early Cancer Diagnostics," Industrial Research 2009 (Grant BANP) Fondo Investimenti per la Ricerca di Base RBAP11BYNP (Newton) (to F. B.), and University of Torino-Compagnia di San Paolo Grant RETHE (to F. B.), Grant GeneRNet (to M. A.), FP7-ICT-2011-8 Biloba (contract 318035), and Consiglio Nazionale delle Ricerche grant "Personalized Medicine" (to F. B.).

The abbreviations used are:

ECM extracellular matrix
NLGNs neuroligins
Ecs endothelial cells
BM basement membrane
VEGF-A vascular endothelial growth factor A
BME basal membrane extract
Dll4 δ-like ligand 4
qRT quantitative RT
DPBS Dulbecco's PBS
ANOVA analysis of variance
GFAP glial fibrillary acid protein
P postnatal.

REFERENCES

1. Davis, G. E., and Senger, D. R. (2005) Endothelial extracellular matrix biosynthesis, remodeling, and functions during vascular morphogenesis and neovessel stabilization. Circ. Res. 97, 1093–1107
2. Kalluri, R. (2003) Basement membranes: structure, assembly and role in tumour angiogenesis. Nat. Rev. Cancer 3, 422–433
3. Ribatti, D., and Crivellato, E. (2012) "Sprouting angiogenesis," a reappraisal. Dev. Biol. 372, 157–165
4. Estrach, S., Cailleteau, L., Franco, C. A., Gerhardt, H., Stefani, C., Lemichez, E., Gagnoux-Palacios, L., Meneguzzi, G., and Mettouchi, A. (2011) Laminin-binding integrins induce Dll4 expression and notch signaling in endothelial cells. Circ. Res. 109, 172–182
5. Dejana, E. (1996) Endothelial adherens junctions: implications in the control of vascular permeability and angiogenesis. J. Clin. Invest. 98, 1949–1953
6. Craig, A. M., and Kang, Y. (2007) Neurexin-neuroligin signaling in synapse development. Curr. Opin. Neurobiol. 17, 43–52
7. Bottos, A., Destro, E., Rissone, A., Graziano, S., Cordara, G., Assenzio, B., Cera, M. R., Mascia, L., Bussolino, F., and Arese, M. (2009) The synaptic proteins neurexins and neuroligins are widely expressed in the vascular system and contribute to its functions. Proc. Natl. Acad. Sci. U.S.A. 106, 20782–20787

8. Rissone, A., Foglia, E., Sangiorgio, L., Cermenati, S., Nicoli, S., Cimbro, S., Beltrame, M., Bussolino, F., Cotelli, F., and Arese, M. (2012) The synaptic proteins _-neurexin and neuroligin synergize with extracellular matrixbinding vascular endothelial growth factor A during zebrafish vascular development. Arterioscler. Thromb. Vasc. Biol. 32, 1563–1572
9. Bedell, V. M., and Ekker, S. C. (2012) Nervy vasculature. Arterioscler. Thromb. Vasc. Biol. 32, 1546–1547
10. Gerhardt, H., Golding, M., Fruttiger, M., Ruhrberg, C., Lundkvist, A., Abramsson, A., Jeltsch, M., Mitchell, C., Alitalo, K., Shima, D., and Betsholtz Betsholtz, C. (2003) VEGF guides angiogenic sprouting utilizing endothelial tip cell filopodia. J. Cell Biol. 161, 1163–1177
11. Stalmans, I., Ng, Y. S., Rohan, R., Fruttiger, M., Bouché, A., Yuce, A., Fujisawa, H., Hermans, B., Shani, M., Jansen, S., Hicklin, D., Anderson, D. J., Gardiner, T., Hammes, H. P., Moons, L., Dewerchin, M., Collen, D., Carmeliet, P., and D'Amore, P. A. (2002) Arteriolar and venular patterning in retinas of mice selectively expressing VEGF isoforms. J. Clin. Invest. 109, 327–336
12. Nikolopoulos, S. N., Blaikie, P., Yoshioka, T., Guo, W., and Giancotti, F. G. (2004) Integrin _4 signaling promotes tumor angiogenesis. Cancer Cell 6, 471–483
13. Varoqueaux, F., Aramuni, G., Rawson, R. L., Mohrmann, R., Missler, M., Gottmann, K., Zhang, W., Südhof, T. C., and Brose, N. (2006) Neuroligins determine synapse maturation and function. Neuron 51, 741–754
14. Kennel, S. J., Epler, R. G., Lankford, T. K., Foote, L. J., Dickas, V., Canamucio, M., Cavalierie, R., Cosimelli, M., Venturo, I., and Falcioni, R. (1990) Second generation monoclonal antibodies to the human integrin _6_4. Hybridoma 9, 243–255
15. Primo, L., Seano, G., Roca, C., Maione, F., Gagliardi, P. A., Sessa, R., Martinelli, M., Giraudo, E., di Blasio, L., and Bussolino, F. (2010) Increased expression of _6 integrin in endothelial cells unveils a proangiogenic role for basement membrane. Cancer Res. 70, 5759–5769
16. Sawamiphak, S., Ritter, M., and Acker-Palmer, A. (2010) Preparation of retinal explant cultures to study ex vivo tip endothelial cell responses. Nat. Protoc. 5, 1659–1665
17. Tsai, W.-H. (1985) Moment-preserving thresolding: a new approach. Comp. Vis. Graph. Image Proc. 29, 377–393
18. Gariano, R. F., and Gardner, T. W. (2005) Retinal angiogenesis in development and disease. Nature 438, 960–966
19. Hellström, M., Phng, L. K., Hofmann, J. J., Wallgard, E., Coultas, L., Lindblom, P., Alva, J., Nilsson, A. K., Karlsson, L., Gaiano, N., Yoon, K., Rossant, J., Iruela-Arispe, M. L., Kalén, M., Gerhardt, H., and Betsholtz, C. (2007) Dll4 signalling through Notch1 regulates formation of tip cells during angiogenesis. Nature 445, 776–780
20. Yáñez-Mó, M., Alfranca, A., Cabañas, C., Marazuela, M., Tejedor, R., Ursa, M. A., Ashman, L. K., de Landázuri, M. O., and Sánchez-Madrid, F. (1998) Regulation of endothelial cell motility by complexes of tetraspan molecules CD81/TAPA-1 and CD151/PETA-3 with _3_1 integrin localized at endothelial lateral junctions. J. Cell Biol. 141, 791–804
21. Georges-Labouesse, E., Messaddeq, N., Yehia, G., Cadalbert, L., Dierich, A., and Le Meur, M. (1996) Absence of integrin _6 leads to epidermolysis bullosa and neonatal death in mice. Nat. Genet. 13, 370–373
22. Germain, M., De Arcangelis, A., Robinson, S. D., Baker, M., Tavora, B., D'Amico, G., Silva, R., Kostourou, V., Reynolds, L. E., Watson, A., Jones, J. L., Georges-Labouesse, E., and Hodivala-Dilke, K., (2010) Genetic ablation of the _6-integrin subunit in Tie1Cre mice enhances tumour angiogenesis. J. Pathol. 220, 370–381
23. Hallmann, R., Horn, N., Selg, M., Wendler, O., Pausch, F., and Sorokin, L. M. (2005) Expression and function of laminins in the embryonic and mature vasculature. Physiol. Rev. 85, 979–1000
24. Stenzel, D., Franco, C. A., Estrach, S., Mettouchi, A., Sauvaget, D., Rosewell, I., Schertel, A., Armer, H., Domogatskaya, A., Rodin, S., Tryggvason, K., Collinson, L., Sorokin, L., and Gerhardt, H. (2011) Endothelial basement membrane limits tip cell formation by inducing Dll4/Notch signalling in vivo. EMBO Rep. 12, 1135–1143
25. Ushkaryov, Y. A., Petrenko, A. G., Geppert, M., and Südhof, T. C. (1992) Neurexins: synaptic cell surface proteins related to the_-latrotoxin receptor and laminin. Science 257, 50–56
26. Rudenko, G., Hohenester, E., and Muller, Y. A. (2001) LG/LNS domains: multiple functions-one business end? Trends Biochem. Sci. 26, 363–368

27. Carpentier, G., Martinelli, M., Courty, J., and Cascone, I. (2012) Angiogenesis Analyzer for ImageJ. 4th ImageJ User and Developer Conference proceedings, pp. 198–201, Mondorf-les-Bains, Luxembourg, ISBN 2- 919941-18-6
28. Bolte, S., and Cordelières, F. P. (2006) A guided tour into subcellular colocalization analysis in light microscopy. J. Microsc. 224, 213–232